Cloaking of a vertical cylinder in waves using variable bathymetry

By R. PORTER[1]† AND J. N. NEWMAN[2]

[1]School of Mathematics, University of Bristol, Bristol, BS8 1TW, UK

[2]Department of Mechanical Engineering, MIT, Cambridge, MA 02139, USA

(Received ?; revised ?; accepted ?. - To be entered by editorial office)

The paper describes a process which allows a vertical circular cylinder subject to plane monochromatic surface gravity waves to appear invisible to the far-field observer. This is achieved by surrounding the cylinder with an annular region of variable bathymetry. Two approaches are taken to investigate this effect. First a mild-slope approximation is applied to the governing linearised three-dimensional water wave equations to formulate a depth-averaged two-dimensional wave equation with varying wavenumber over the variable bathmetry. This is then solved by formulating a domain integral equation, solved numerically by discretisation. For a given set of geometrical and wave parameters, the bathymetry is selected by a numerical optimisation process and it is shown that the scattering cross-section is reduced towards zero with increasing refinement of the bathymetry. A fully three-dimensional boundary element method, based on the WAMIT solver but adapted here to allow for depressions in the bed, is used to assess the accuracy of the mild-slope results and then further numerically optimise the bathymetry towards a cloaking structure. Numerical results provide strong evidence that perfect cloaking is possible for the fully three-dimensional problem. One practical application of the results is that cloaking implies a reduced mean drift force on the cylinder.

1. Introduction

The idea of rendering objects placed in a wave field to appear invisible to the far-field observer has been given the name 'cloaking'. Attempts at cloaking using absorbing and anti-reflection devices extend back over many decades, mainly applied to the area of electromagnetic theory. Interest in this subject was re-ignited by the simultaneous publications of Pendry *et al.* (2006) and Leonhardt (2006), both of whom showed the principle of a perfect cloaking mechanism. The concept of Pendry *et al.* (2006) uses the invariance of Maxwell's equations for electromagnetism under a change of coordinate system, provided the material parameters (permittivity and permeability) are suitably rescaled (Ward & Pendry (1996)). Leonhardt (2006) applied essentially the same principle in a two-dimensional geometric optics setting through the use of conformal mappings. The invariance property of the governing equations allows mappings to be constructed from a problem in which waves propagate uninterrupted through free space into a problem with a circular (in two dimensions) or spherical (in three dimensions) inclusion surrounded by an annular region with varying material parameters. Plane waves incident on the annular region are bent by the varying anisotropic refracted index of the material (being a simple function of the perimittivity and permeability) so that the wave fronts deflect

† Corresponding author. Email: richard.porter@bris.ac.uk

seemlessly around the inclusion without entering it. By construction the annular region, including its interior and exterior boundaries, is reflectionless. Waves from behind some arbitrary object placed within the inclusion are bent around the object reforming without a phase shift on the other side of the object. Thus, the annular region is called a 'cloak'. In electromagnetics the cloak requires construction from materials with a large range of continuously varying anisotropic refractive index – belonging to a class of so-called metamaterials. A perfect cloak (one with no scattering cross section) is practically impossible to achieve because of singular points in the mapping at which the refractive index becomes unbounded. The dispersive nature of waves propagating within the cloak implies that cloaking is tuned to specific frequencies and is, in general, not broadbanded.

The concept of cloaking has been applied to other physical wave systems, most notably to waves in an acoustic fluid where a similar mapping technique can be formulated in both two and three dimensions – see Cummer & Schurig (2007), Chen & Chan (2007) and Cummer *et al.* (2007). Now the density and bulk modulus of a cloaking material surrounding the inclusion must be designed to vary in a particular manner, determined by the mapping, to deflect waves around the device.

In three-dimensional elasticity, Milton *et al.* (2006) showed that Navier's elasticity equations are not invariant under a coordinate transformation although Farhat *et al.* (2009) have shown that in thin two-dimensional elastic Euler-Bernoulli plates a mapping technique can be used to effect a cloaking device.

There is more limited work in the area of cloaking for surface waves on a fluid, perhaps because the scope for physical application is limited. Farhat *et al.* (2008) studied surface waves in the gravity-capillary lengthscale, using a cloak comprised of an annular domain containing a large periodic array of small vertical circular posts. Here, the incident wavelength is large compared to the dimension of the posts in the cloaking device, though small compared to the inclusion being cloaked. Established homogenisation techniques are used to capture the effect of the posts in a continuum model which includes the components of anisotropy required of a model cloak derived under the transformation technique. Farhat *et al.* (2008) were then able to design the structure of the array of posts to achieve the correct radial behaviour of their anisotropic shear modulus tensor although admitted that an extra degree of flexibility needed for the design of a perfect cloak, that of radially varying density, was not possible under the homogenisation model. Nevertheless, experiments are presented alongside the theory showing the cloak to be effective. A second paper, Alam (2012), shows how cloaking of an object floating in the surface can be achieved in a two-dimensional setting in the presence of a two-layer stratified fluid, using a series of sinuisoidal bottom corrugations to transfer energy from incoming surface waves into interfacial waves which pass below the surface object before being transformed back into surface waves by by another series of bottom corrugations on the other side of the object.

In this paper we consider the cloaking of a cylinder by surface waves on a fluid. Specifically, we consider using changes in the fluid depth as a mechanism for cloaking a vertical circular cylinder. Thus, it is well known that surface waves are refracted by changes in depth. To see how refractive effects enter a model of wave propagation, consider the shallow water wave equations for the free-surface elevation $\mathrm{Re}\{\eta(x,y)\mathrm{e}^{-\mathrm{i}\omega t}\}$ (see Mei (1983) for example) as a function of the two horizontal coordinates x, y and time t where ω is an assumed radian frequency. Then η is determined as the solution to

$$\nabla.(h\nabla\eta) + k_0^2 h_0 \eta = 0 \tag{1.1}$$

where $\omega^2/(gh_0) = k_0^2$, g is gravity and $h = h(x, y)$. Using $\eta = h^{-1/2}u$ in (1.1) gives

$$(\nabla^2 + k_0^2 n^2)u = 0, \qquad n^2 = \left(\frac{h_0^2}{h^2} + \frac{(\nabla h)^2}{4(kh)^2}\right) \tag{1.2}$$

where n is a refractive index which varies with h, and $k^2 = \omega^2/(gh)$ defines a local wavenumber. Equation (1.2) is valid only in the long wave limit $kh \ll 1$ and if $|\nabla h/kh| \ll 1$. A more sophisticated depth-averaged model gives rise to the mild-slope equations and formally extends the model (1.2) over all values of kh at the expense of a more complicated definition of n whilst the 'mild slope' restriction $|\nabla h/kh| \ll 1$ remains in place.

The same assumption, $|\nabla h/kh| \ll 1$, is used in developing the ray theory for short wavelengths ($kh \gg 1$), or geometric optic limit. This leads to the Eikonal equation for a function $S(x, y)$ representing lines of constant wave phase, which can be expressed as

$$|\nabla S| = k(h) \tag{1.3}$$

(see, for example, Mei (1983)) where again k varies locally with h now according to the dispersion relation, $\omega^2/g = k \tanh kh$. The equation (1.3) appears to provide a further motivation to using changes in depth to effect cloaking. Thus, we can imagine prescribing $S(x, y)$ such that the ray paths (perpendicular to lines of constant phase) are directed around a circular cylinder and use (1.3) as a method for determining h via an inverse procedure. For example, choosing $S = k_0(r + a^2/r)\cos\theta$, expressed in usual polar coordinates, satisfies the two essential requirements on the function S for cloaking: (i) $\partial_r S = 0$ on $r = a$; and (ii) $S \to k_0 x$ as $r \to \infty$. These state that lines of constant phase: (i) are perpendicular to the boundary of the cylinder of radius a; and (ii) coincide with x equals a constant far away from the cylinder. Hence parallel incident ray paths from infinity in a fluid of depth h_0 are deflected locally around the cylinder. Pursuing this inverse procedure produces regions fore and aft of the cylinder where h is undefined. This difficulty persists for more exotic functions S satisfying conditions (i) and (ii). Thus the dispersion relation does not offer enough contrast in refractive indices through changes in depth to bend incident rays around the cylinder and create a perfect (or near perfect) cloak.

Efforts to apply the coordinate transformation method described previously to the linearised water wave problem also seem unlikely to succeed. There are two issues. First, although it is possible to envisage a physical problem in which the depth is anisotropic (for example, the depth profile of the bed could be comprised of interleaving narrow vertical combs whose profiles in the radial and azimuthal directions may be different) the fact remains that the transformation method (whose map is not area preserving) requires two 'material' parameters to be varying in the domain and here we may only control the depth. Second, whilst the governing field equation (Laplace's equation) can be preserved under a conformal mapping of the horizontal coordinates, the required rescaling of the vertical coordinate implies that the boundary conditions on the free surface and the bottom bed are not preserved. This obstacle seems particular to the water-wave problem, since lateral boundary conditions do not exist in the other problems cited previously for other types of wave fields.

Given the preceeding arguments it seems unlikely that a cloak can be designed for surface waves in a homogeneous fluid by varying the fluid depth. Thus we have moved back from what is now usually defined as cloaking in which a 'dead zone', devoid of fluid motion and waves, is created and within which an object of arbitrary shape can be hidden from the far-field observer. Instead, we focus on the question of whether it is possible to cloak an object of a specific shape having a specific boundary condition upon its surface. This is analogous to the idea used by Alù & Enghata (2005), whose work preceeded Pendry *et al.* (2006) and Leonhardt (2006), who considered cloaking

of TM or TE polarised electromagnetic waves by surrounding a dielectric cylinder with given permittivity and permeability with an annular region of a different (but constant) permittivity and permeability. Alù & Enghata (2005) showed that, for large wavelength-to-cylinder ratios, low visibility could be obtained at certain frequencies. They appealed to the idea that, in this limit, the uncloaked cylinder scattering pattern is predominantly a dipolar and that a destructive interference effect could be introduced by adding an annular cloaking domain with appropriately-chosen dielectric constants. This idea lends itself well to surface gravity waves which are typically thought of as long compared to the size of a typical scattering object. We use a vertical circular cylinder extending throughout the depth as the scattering object, mainly because of its simplicity, although we are not suggesting that this is the only object that we could have chosen. Surrounding the cylinder is an annular region of varying bathymetry which is described by a finite expansion of orthogonal functions in the radial and azimuthal directions. By adjusting the weighting of each component of the bathymetry via a numerical optimisation process, we aim to lower the scattering cross section from the uncloaked cylinder with a limit of zero representing the perfect cloak.

The outline of the rest of the paper is as follows. In Section 2, we give a statement of the problem of a cylinder surrounded by varying bathymetry. In Section 3 an approximation based on the mild-slope equation (MSE) is described, in which the complexity of the fully three-dimensional boundary-value problem is reduced by depth-averaging to a simpler two-dimensional wave equation with a spatially-varying wavenumber. A domain integral equation is derived, adapting recent work by Griffiths & Porter (2012) to account for the cylinder. Section 4 describes a fully three-dimensional boundary element method which is based on an adaptation of the WAMIT solver† to account for depressions in the bed below the depth at infinity. The numerical optimisation process used for cloaking and comparisons between the results from MSE and full linear theory are made in Section 5.

The paper thus attempts to describe the process by which this problem arose and evolved, being instigated by the MSE approach (Porter (2011)) and pursued by (Newman (2012)) using a fully three-dimensional theory to validate and refine the MSE results. Some significant changes to the methods and results have emerged since those initial conference proceedings were published. In particular, there is a greater emphasis here on axisymmetric beds which were overlooked in earlier work. A discussion of the practical use of cloaking as a possible means of reducing mean drift forces on vertical cylinders is also included.

2. Formulation of the problem

We adopt cylindrical polar coordinates (r, θ, z) with $z = 0$ coinciding with the mean free surface of the fluid and z pointing vertically upwards. An impermeable vertical cylinder of constant circular cross section of radius a is centred along the z-axis and extends throughout the depth. The sea-bed is defined by $z = -h(\boldsymbol{r})$ for $r > a$, with $\boldsymbol{r} = (r, \theta)$. Here $h(\boldsymbol{r})$ is a continuous function with continuous derivatives, and $h(\boldsymbol{r}) = h_0$, a constant, for $r > b$. Thus, the bed is allowed to vary in the annular region $a < r < b$.

We adopt linearised water wave theory in which the velocity potential is given by $\mathrm{Re}\{\Phi(\boldsymbol{r}, z)\mathrm{e}^{-\mathrm{i}\omega t}\}$ where ω is the assumed angular frequency of motion. Then Φ satisfies

$$(\nabla^2 + \partial_{zz})\Phi = 0, \quad -h(\boldsymbol{r}) < z < 0, \ r > a, \ 0 \leqslant \theta < 2\pi, \tag{2.1}$$

† www.wamit.com

where $\nabla = (\partial_r, r^{-1}\partial_\theta)$,

$$\Phi_z - K\Phi = 0, \quad \text{on } z = 0,\ r > a, \tag{2.2}$$

where $K = \omega^2/g$, g is gravitational acceleration and

$$\Phi_z + \nabla h.\nabla\Phi = 0, \quad \text{on } S_b := \{z = -h(\boldsymbol{r}),\ r > a\}, \tag{2.3}$$

which reduces to $\Phi_z = 0$, on $z = -h_0$ for $r > b$. On the cylinder, $\boldsymbol{r} = \boldsymbol{r}_a = (a, \theta)$ we have

$$\Phi_r(\boldsymbol{r}_a, z) = 0, \quad \text{on } S_c := \{-h(\boldsymbol{r}_a) < z < 0,\ 0 \leqslant \theta < 2\pi\}\ . \tag{2.4}$$

An incident wave propagating in the direction β is given by the potential

$$\Phi_{inc}(\boldsymbol{r}, z) = \mathrm{e}^{\mathrm{i}k_0 r\cos(\theta-\beta)} w(k_0h_0, k_0z), \tag{2.5}$$

where

$$w(p, q) = \frac{\cosh(p+q)}{\cosh p}, \tag{2.6}$$

and $k = k_0$ is the real positive root corresponding to $h = h_0$ of

$$k\tanh kh = K. \tag{2.7}$$

The total potential is $\Phi = \Phi_{inc} + \Phi_{sc}$ where Φ_{sc} is a potential representing the scattered waves which therefore satisfies the radiation condition and hence

$$\Phi_{sc}(\boldsymbol{r}, z) \sim \mathcal{A}(\theta;\beta)\sqrt{\frac{2}{\pi k_0 r}}\,\mathrm{e}^{\mathrm{i}(k_0r-\pi/4)} w(k_0h_0, k_0z), \qquad \text{as } k_0r \to \infty \tag{2.8}$$

where $\mathcal{A}(\theta;\beta)$ measures the circular scattered wave amplitude in the direction θ due to a wave incident in the direction β. The dependence of various quantities on β is made explicit where later reference is required.

In order that the cylinder be cloaked it is required that $A(\theta;\beta) \equiv 0$ for $0 \leqslant \theta < 2\pi$. Alternatively, the total energy scattered to infinity (the scattering cross section)

$$\mathcal{E} = \frac{1}{2\pi}\int_0^{2\pi} |\mathcal{A}(\theta;\beta)|^2 \mathrm{d}\theta = -\mathrm{Re}\{\mathcal{A}(\beta;\beta)\} \tag{2.9}$$

must be zero. The final equality in (2.9) is a well-known result originally derived by Maruo (1960) in the water-wave context. In other contexts it is known as the optical theorem.

If $h(\boldsymbol{r}) = h_0$ for all $r > a$ so the bed is flat everywhere, then the exact solution is well-known (e.g. Mei (1983)) and given by

$$\Phi_{cyl}(\boldsymbol{r}, z) = \psi_{cyl}(\boldsymbol{r};\beta) w(k_0h_0, k_0z), \tag{2.10}$$

where

$$\psi_{cyl}(\boldsymbol{r};\beta) = \sum_{n=-\infty}^{\infty} \mathrm{i}^n \left(J_n(k_0r) - Z_nH_n(k_0r)\right)\mathrm{e}^{\mathrm{i}n(\theta-\beta)}. \tag{2.11}$$

Here J_n and $H_n \equiv H_n^{(1)}$ are Bessel and Hankel functions, and $Z_n = J_n'(k_0a)/H_n'(k_0a)$. Thus the scattering amplitude for the flat bed is given by

$$\mathcal{A}_{cyl}(\theta;\beta) = -\sum_{n=-\infty}^{\infty} Z_n \mathrm{e}^{\mathrm{i}n(\theta-\beta)}. \tag{2.12}$$

The total scattered wave energy (2.9) equates to

$$\mathcal{E}_{cyl} = \sum_{n=-\infty}^{\infty} |Z_n|^2 = \mathrm{Re}\left\{\sum_{n=-\infty}^{\infty} Z_n\right\}, \tag{2.13}$$

which is independent of β as expected, and never zero.

3. The mild-slope approximation

In this section the problem formulated in Section 2 is approximated by employing the mild-slope method. That is, the potential locally assumes the depth-dependence assigned to propagating modes over a locally flat bed of the same depth,

$$\Phi(\boldsymbol{r},z)\approx\phi(\boldsymbol{r})w(kh,kz), \tag{3.1}$$

in which $k(\boldsymbol{r})=k(h)$ denotes the positive, real root of (2.7) and the depth, $h(\boldsymbol{r})$ is now varying spatially. We follow the implementation of the approximation (3.1) of Chamberlain & Porter (1995) which uses a variational principle to replace (2.1), (2.2) and (2.3) by the single modified mild-slope equation (MMSE), namely

$$\nabla\cdot(u_0\nabla\phi)+(k_0^2u_0+u_1\nabla^2h+u_2(\nabla h)^2)\phi=0,\qquad r>a \tag{3.2}$$

where $u_0(h)=\mathrm{sech}^2kh(2kh+\sinh 2kh)/(4k)$ and $u_1(h)$, $u_2(h)$ are given by Chamberlain & Porter (1995) but are not required explicitly here. In addition, the boundary condition (2.4) on the cylinder gives rise, from the variational principle, to the natural condition requiring

$$\int_{-h}^{0}w\,\frac{\partial(w\phi)}{\partial r}\bigg|_{r=a}\mathrm{d}z=0,\qquad 0\leqslant\theta<2\pi. \tag{3.3}$$

After integrating, this gives the (rather unintuitive) boundary condition on the reduced potential ϕ to be

$$u_0\phi_r+u_1h_r\phi=0,\qquad \text{on } r=a. \tag{3.4}$$

This condition is overlooked in later work of Chamberlain & Porter (1999) and also in Porter (2011), but is taken into account in a recent paper of Liu *et al.* (2013).

A transformation of (3.2) into its canonical form is achieved by writing

$$\phi(\boldsymbol{r})=\{u_0(h_0)/u_0(h(\boldsymbol{r}))\}^{1/2}\psi(\boldsymbol{r}), \tag{3.5}$$

upon which ψ can be shown to satisfy (e.g. Griffiths & Porter (2012))

$$\nabla^2\psi+\kappa(\boldsymbol{r})\psi=0,\quad r>a, \tag{3.6}$$

where

$$\kappa(\boldsymbol{r})=k_0^2+A(h)\nabla^2h+B(h)(\nabla h)^2, \tag{3.7}$$

and $A(h)$, $B(h)$ are now functions of u_0, u_1 and u_2. With the abbreviation $\mathcal{K}=2k(h)h$, these factors are given explicitly (see, for example, Griffiths & Porter (2012)) by

$$\begin{aligned}A(h)&=-2k/(\mathcal{K}+\sinh\mathcal{K}),\\ B(h)&=k^2\{\mathcal{K}^4+4\mathcal{K}^3\sinh\mathcal{K}+3\mathcal{K}^2(2\cosh^2\mathcal{K}+1)+\\ &\qquad 18\mathcal{K}\sinh\mathcal{K}+3\sinh^2\mathcal{K}(2\cosh\mathcal{K}+5)\}/\{3(\mathcal{K}+\sinh\mathcal{K})^4\}.\end{aligned}$$

Application of (3.5) to (3.4) leads to the boundary condition

$$\psi_r+h_rA(h)\psi=0,\qquad \text{on } r=a,\ 0\leqslant\theta<2\pi. \tag{3.8}$$

Finally we mimic the decomposition of Φ writing $\psi(\boldsymbol{r})=\psi_{inc}(\boldsymbol{r})+\psi_{sc}(\boldsymbol{r})$ where $\psi_{inc}(\boldsymbol{r})=\mathrm{e}^{\mathrm{i}k_0r\cos(\theta-\beta)}$, and

$$\psi_{sc}(\boldsymbol{r})\sim\mathcal{A}(\theta;\beta)\sqrt{\frac{2}{\pi k_0r}}\,\mathrm{e}^{\mathrm{i}(k_0r-\pi/4)}. \tag{3.9}$$

We briefly remark that the reduced potential ψ_{cyl} defined in (2.12) and used to express the solution of the exact scattering by a circular cylinder on a flat bed is also (and unsurprisingly) an exact solution of the MMSE with $\mathcal{A}(\theta;\beta)$ replaced by $\mathcal{A}_{cyl}(\theta;\beta)$ as defined in (2.13).

We now follow closely the method described in Griffiths & Porter (2012), reformulating the wave equation (3.6) into an integral equation using a Green function $G(\boldsymbol{r};\boldsymbol{r}')$ satisfying

$$(\nabla^2 + k_0^2)G = \delta(\boldsymbol{r}-\boldsymbol{r}'), \tag{3.10}$$

with $\boldsymbol{r}'$ representing the field point (r',θ') and $G_r(\boldsymbol{r}_a;\boldsymbol{r}')=0$. It can readily be shown that

$$G(\boldsymbol{r};\boldsymbol{r}') = -\frac{\mathrm{i}}{4}H_0(k_0\rho) + \frac{\mathrm{i}}{4}\sum_{n=-\infty}^{\infty} Z_n H_n(k_0 r)H_n(k_0 r')\mathrm{e}^{\mathrm{i}n(\theta-\theta')}, \tag{3.11}$$

where $\rho^2 = |\boldsymbol{r}-\boldsymbol{r}'|^2 \equiv r^2 + r'^2 - 2rr'\cos(\theta-\theta')$ and with Z_n defined following (2.11). The result applying Green's identity to $\psi - \psi_{cyl}$ and G over the infinite domain $r > a$, $0 \leqslant \theta < 2\pi$ is

$$\begin{aligned}\psi(\boldsymbol{r}') + \iint_D [\kappa(\boldsymbol{r}) - k_0^2]G(\boldsymbol{r};\boldsymbol{r}')\psi(\boldsymbol{r})\, r\mathrm{d}r\mathrm{d}\theta \\ - \int_0^{2\pi} A(h(\boldsymbol{r}_a))h_r(\boldsymbol{r}_a)G(\boldsymbol{r}_a;\boldsymbol{r}')\psi(\boldsymbol{r}_a)a\mathrm{d}\theta = \psi_{cyl}(\boldsymbol{r}';\beta),\end{aligned} \tag{3.12}$$

for $|\boldsymbol{r}'| \geqslant a$, where ψ_{cyl} is defined by (2.11) and $D := \{a < r < b,\ 0 < \theta < 2\pi\}$ is the projection of the varying bed S_b onto the (r,θ)-plane. The boundary integral on $\partial D := \{r = a,\ 0 \leqslant \theta < 2\pi\}$ appears during the application of (3.8). Thus (3.12) serves as an integral equation for the unknown ψ when $\boldsymbol{r}'$ is restricted to $D \cup \partial D$ and defines ψ beyond D once ψ is known in $D \cup \partial D$.

Taking $k_0 r' \to \infty$ allows us to access the far-field behaviour of ψ which, in comparison with (3.9), gives

$$\begin{aligned}\mathcal{A}(\theta';\beta) = \mathcal{A}_{cyl}(\theta';\beta) + \frac{\mathrm{i}}{4}\iint_D [\kappa(\boldsymbol{r}) - k_0^2]\psi_{cyl}(\boldsymbol{r};\theta'+\pi)\psi(\boldsymbol{r})\, r\mathrm{d}r\mathrm{d}\theta \\ - \frac{\mathrm{i}}{4}\int_0^{2\pi} A(h(\boldsymbol{r}_a))h_r(\boldsymbol{r}_a)\psi_{cyl}(\boldsymbol{r}_a;\theta'+\pi)\psi(\boldsymbol{r}_a)\, a\mathrm{d}\theta,\end{aligned} \tag{3.13}$$

where $\mathcal{A}_{cyl}$ is defined by (2.12). In deriving the above, we have made use of the leading-order large-argument expansion of the Hankel function in (3.11).

The strategy is to determine solutions $\psi(\boldsymbol{r})$ over $\boldsymbol{r} \in D \cup \partial D$ from (3.12) and use this to calculate $\mathcal{A}(\theta';\beta)$ from (3.13). Finally, the scattering cross-section $\mathcal{E}$ can be found using (2.9).

The free-surface elevation due to an incident wave of unit amplitude is given by $\eta(\boldsymbol{r}) = (\mathrm{i}/g)\Phi_z(\boldsymbol{r},0)$, which can be accessed from (3.1), (3.5).

Solutions to (3.12) are approximated numerically using a discretisation approach similar to that described by (Griffiths & Porter 2012, section 4.2), thereby allowing the scattering coefficients to be approximated from (3.13). The approximation method is unsophisticated and uses piecewise-constant values for the unknown ψ on an N by M polar grid over the annular domain $D \cup \partial D$. However, the approximation to the integral equations is based on Galerkin's method, and therefore converges rapidly with increasing values of N and M. Nevertheless, the procedure is numerically intensive, requiring the inversion of full $MN \times NM$ matrices. Symmetries in the bathymetry can be exploited

to reduce the domain of the integral equation to a quarter of its original size and this improves the numerical efficiency.

In the particular case where the bathymetry is axisymmetric, with some additional effort, the MSE problem can be reformulated by expanding unknown quantities into Fourier modes. This leads to a series of simpler one-dimensional integral equations for each azimuthal mode involving non-singular Green functions. Not only is this much quicker to implement numerically but it also allows the MSE results to be validated against the full system when axisymmetry has not been assumed. The results have also been validated against those produced by the method of Griffiths & Porter (2012) for the case of no cylinder, by letting the radius of the circular cylinder shrink towards zero. Further validation against fully three-dimensional calculations will follow in §5.

4. Fully three-dimensional calculations

In a fluid of constant depth the scattering characteristics of a body can be analyzed using the panel method (see, for example, Lee & Newman (2004)). A boundary integral equation for the unknown velocity potential is derived, using the Green function which satisfies the boundary conditions on the free surface and bottom and the radiation condition in the far field. The domain of the integral equation is restricted to the submerged surface S of the body. After discretization the integral equation is reduced to a linear system of algebraic equations. This method can be extended to cases with variable bathymetry where $h(x, y) \leqslant h_0$, by extending S to include S_b the bottom in the region of varying depth. Ferreira & Newman (2009) used this approach to analyze wave effects on a ship above a sloping bottom. However it cannot be used if $h(x, y) > h_0$, as is the case for bathymetry suggested by results indicated by the MSE approach later in Section 5, since the Green function which satisfies the boundary condition on $z = -h_0$ is singular if $z < -h_0$. This restriction could be avoided by using a different Green function, e.g. corresponding to the maximum depth or infinite depth, but the resulting computational domain would include the entire bottom extending to infinity. Instead we consider a more efficient approach based on domain decomposition, with a matching boundary between the interior domain with variable bathymetry and the exterior domain with constant depth. Matching boundaries have been used for a variety of wave-body problems, especially for cases involving thin vertical barriers and bodies with vertical sides. Belibassakis (2008) and Pinkster (2011) have used matching with panel methods to analyze problems with other types of bathymetry.

Two domains D_i $(i = 0, 1)$ are considered, with the corresponding velocity potentials denoted by $\Phi^{(i)}$. The exterior domain D_0 extends to infinity, with constant depth h_0. In the interior domain D_1 the depth $h(x, y)$ is arbitrary, except that it must match the depth h_0 on the matching boundary, S_m. The boundary surface of D_1, not including the free surface, is $S_1 = S_c \cup S_b \cup S_m$ where S_c denotes the wetted surface of the vertical cylinder and S_b represents the varying bed within D_1. The potential $\Phi^{(0)}$ includes the incident wave Φ_{inc} defined by (2.5) and the scattering component Φ_{sc} which satisfies the radiation condition in the far field given by (2.8). The matching boundary S_m separates the two domains, extending from the bottom $z = -h_0$ to the free surface $z = 0$. The unit normal is defined to point out of the domain D_i on its boundary.

Green's second identity is applied separately in each domain. Thus for field points $\boldsymbol{x}$

on the boundary surface S_i,

$$2\pi\Phi^{(i)}(\boldsymbol{x})+\iint_{S_i}\left(\Phi^{(i)}(\boldsymbol{\xi})\frac{\partial G^{(i)}(\boldsymbol{\xi};\boldsymbol{x})}{\partial n_{\boldsymbol{\xi}}}-G^{(i)}(\boldsymbol{\xi};\boldsymbol{x})\frac{\partial\Phi^{(i)}(\boldsymbol{\xi})}{\partial n_{\boldsymbol{\xi}}}\right)\mathrm{d}S_{\boldsymbol{\xi}}=\begin{cases}4\pi\Phi_{inc}(\boldsymbol{x}), & i=0,\\ 0, & i=1.\end{cases} \tag{4.1}$$

Here $G^{(1)}(\boldsymbol{\xi};\boldsymbol{x})$ is any Green function which is regular within D_1 (except at the source point $\boldsymbol{\xi}$, where $G^{(1)}\sim 1/|\boldsymbol{\xi}-\boldsymbol{x}|$), and satisfies the free-surface condition. For simplicity the conventional free-surface Green function for infinite depth is used. $G^{(0)}$ is the Green function for finite depth, h_0. For the specification of both types of Green function see Mei (1983). The term $4\pi\Phi_{inc}$ is included on the right-hand side since $\Phi^{(0)}$ does not satisfy the radiation condition.

On S_b and S_c (2.3) and (2.4) hold and so the normal velocity $\Phi_n^{(1)}=0$, where the subscript n denotes the normal derivative. The appropriate boundary conditions on S_m are $\Phi^{(0)}=\Phi^{(1)}$ and $\Phi_n^{(0)}=-\Phi_n^{(1)}$, expressing continuity of pressure and normal velocity respectively. Using (4.1), writing separate equations for the two domains and invoking the boundary conditions on S_m gives the following three equations:

$$2\pi\Phi^{(1)}+\iint_{S_b\cup S_c}\Phi^{(1)}G_n^{(1)}\mathrm{d}S_{\boldsymbol{\xi}}+\iint_{S_m}\Phi^{(0)}G_n^{(1)}\mathrm{d}S_{\boldsymbol{\xi}}+\iint_{S_m}G^{(1)}\Phi_n^{(0)}\mathrm{d}S_{\boldsymbol{\xi}}=0 \tag{4.2}$$

$$2\pi\Phi^{(0)}+\iint_{S_b\cup S_c}\Phi^{(1)}G_n^{(1)}\mathrm{d}S_{\boldsymbol{\xi}}+\iint_{S_m}\Phi^{(0)}G_n^{(1)}\mathrm{d}S_{\boldsymbol{\xi}}+\iint_{S_m}G^{(1)}\Phi_n^{(0)}\mathrm{d}S_{\boldsymbol{\xi}}=0 \tag{4.3}$$

$$2\pi\Phi^{(0)}+\iint_{S_m}\Phi^{(0)}G_n^{(0)}\mathrm{d}S_{\boldsymbol{\xi}}-\iint_{S_m}G^{(0)}\Phi_n^{(0)}\mathrm{d}S_{\boldsymbol{\xi}}=4\pi\Phi_{inc} \tag{4.4}$$

where (4.2) is applied on $\boldsymbol{x}\in S_b\cup S_c$, and (4.3), (4.4) on $\boldsymbol{x}\in S_m$. In the above equations, arguments have been dropped so that $G_n^{(i)}$ is shorthand for $\partial G^{(i)}(\boldsymbol{\xi};\boldsymbol{x})/\partial n_{\boldsymbol{\xi}}$. The unknowns in (4.2)–(4.4) are $\Phi^{(1)}$ on $S_b\cup S_c$ and $\Phi^{(0)}$, $\Phi_n^{(0)}$ on S_m. The coupled integral equations (4.2)–(4.4) are discretized and solved using a modified version of the panel code WAMIT. The higher-order method is used, with the unknowns represented by B-splines as explained by Lee & Newman (2004). The surfaces S_b and S_c are represented by explicit formulae and S_m is defined to be a circular cylinder of radius b, as in the previous section.

Using $\Phi^{(0)}$ and the function $\mathrm{e}^{-\mathrm{i}k_0r\cos(\theta-\theta')}w(k_0z,k_0h_0)$ in Green's second identity applied to the domain D_0 which extends to infinity, the following relation for the far-field scattering amplitudes can be found

$$\mathcal{A}(\theta';\beta)=-\frac{\mathrm{i}gk_0}{4\omega v_g}\iint_{S_m}\left(\Phi_n^{(0)}-\Phi^{(0)}\frac{\partial}{\partial n}\right)\frac{\cosh\left(k_0(z+h_0)\right)}{\cosh(k_0h_0)}\,\mathrm{e}^{-\mathrm{i}k_0r\cos(\theta-\theta')}\,\mathrm{d}S \tag{4.5}$$

where v_g is the group velocity in depth h_0. In terms of the Kochin function $H(\theta)$ (e.g. Wehausen & Laitone (1963)) the relation $H(\theta)=2\mathrm{i}\mathcal{A}(\theta;\beta)$ holds.

Once $\mathcal{A}(\theta;\beta)$ has been computed from (4.5), the total scattered energy in waves radiated to infinity is computed from (2.9).

Before considering the objective of bathymetry which minimizes the scattered energy, a simpler problem has been considered to validate the procedure described above. A circular cylinder of unit radius is surrounded by an annular bed of constant depth h_1, and the exciting forces acting on the cylinder and on the complete surface $S_b\cup S_c$ are evaluated for a range of wavenumbers and depth ratios h_1/h_0. For $h_1\leqslant h_0$ the results agree to several decimal places with computations using the conventional panel method without domain decomposition. These results are shown in Newman (2012).

5. Numerical results

5.1. *The bathymetry and cloaking procedure*

We are interested in the 'cloaking factor'

$$\mathcal{C} = \frac{\mathcal{E}}{\mathcal{E}_{cyl}}, \tag{5.1}$$

where $\mathcal{E}_{cyl}$ defined by (2.13) is the scattering cross-section for a flat bed and $\mathcal{E}$ is defined for the variable bathymetry by (2.9) with $\mathcal{A}$ defined by (3.13) under the MSE approximation and (4.5) for fully three-dimensional computations. When $\mathcal{C} < 1$, the cylinder with the cloaking region containing the variable bathymetry scatters less energy than with a flat bed. Perfect cloaking requires $\mathcal{C} = 0$.

In order to consider varying bed shapes of a general form, the depth $h(r, \theta)$ is defined by a Fourier-Chebychev basis with

$$h(r,\theta) = h_0 + \sum_{p=1}^{P}\sum_{q=1}^{Q} \alpha_{p,q} f_p(r) \cos(2(q-1)\theta), \tag{5.2}$$

where

$$f_p(r) = \tfrac{1}{2} T_{2p}\left(\frac{b-r}{b-a}\right) - \tfrac{1}{2}(-1)^p, \tag{5.3}$$

and $T_n(\cdot)$ are orthogonal Chebychev polynomials. The particular choice in (5.3) ensures that $h(b, \theta) = h_0$ and $h_r(b, \theta) = 0$ as required by the MSE approach. The expansion in θ dictates that the bed shape is symmetric about both planes $\theta = 0$ and $\theta = \frac{1}{2}\pi$. We have assumed the objective is to cloak for an incident wave angle of $\beta = 0$ and this is most likely to be successful if symmetry is assumed in the bathymetry about the plane $\theta = 0$. Symmetry of the bathymetry in the plane $\theta = \frac{1}{2}\pi$, perpendicular to the assumed wave direction, is motivated by a time-reversibility argument. Suppose a bathymetry cloaks the cylinder for waves from one direction. Reversing time is equivalent to reversing the direction of wave propagation. Consequently, if a cloaking bed were *not* symmetric about a plane perpendicular to the incident wave direction then there would be two cloaking bathymetries, one the mirror image of the other. This seems unlikely although we do not rule this possibility out. It has also been confirmed numerically that the contribution from odd cosine modes play a negligible role in reducing the value of $\mathcal{C}$.

Before considering attempts at cloaking, the resuls from the mild-slope equation (MSE) and full linear theory (FLT) are compared for simple bed shapes. In figures 1(a,b) the variation of $\mathcal{C}$ is shown against $k_0 h_0$ for axisymmetric beds ($Q = 1$) with $a/h_0 = \frac{1}{2}$, $b/h_0 = 5$. In figure 1(a) $P = 1$ has been chosen with $\alpha_{1,1} = 0.1, 0.2, 0.4, 0.8$. Figure 1(b) shows results for $P = 2$, $\alpha_{1,1} = 0$, $\alpha_{2,1} = -0.1, -0.2, -0.4$. A log scale on the vertical axis helps separate results in each figure. The computations from the MSE and FLT are in very good agreement, with only small differences emerging for steeper beds and small values of $k_0 h_0$. These observations are consistent with the range of validity of the MSE and other comparisons between the MSE and full linear theory (see, for example, Ehrenmark *et al.* (2005)).

The procedure used to find the bed shapes leading to the lowest value of $\mathcal{C}$ is now described. In (5.2) the PQ weighting coefficients, $\alpha_{p,q}$, are considered free variables in a numerical optimisation procedure whose objective function is the cloaking factor, $\mathcal{C}$. I.e. the procedure aims to find the minimum value of $\mathcal{C}$ over all $\alpha_{p,q}$ in PQ-dimensional space.

The strategy, followed initially by the MSE approach, increases the number of free pa-

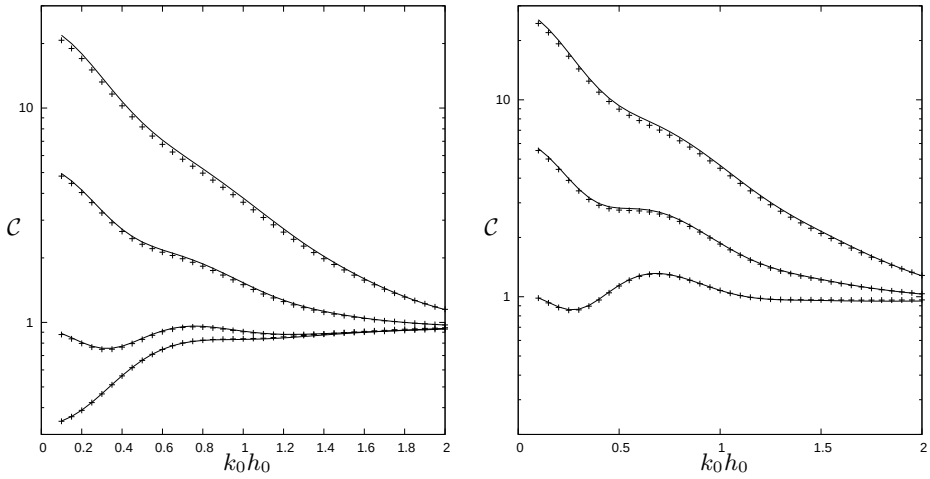

FIGURE 1. Comparison of $\mathcal{C}$ against k_0h_0 computed using MSE (solid lines) and FLT (crosses) for axisymmetric beds with one radial basis mode: (a) $\alpha_{1,1} = 0.1, 0.2, 0.4, 0.8$; (b) $\alpha_{1,1} = 0$, $\alpha_{2,1} = -0.1, -0.2, -0.4$. In both examples, $\mathcal{C}$ increases with increasing magnitude of the coefficients.

rameters (i.e. P and Q) in increments starting with $P = 1$, $Q = 1$ where the optimisation is easily performed. After each optimisation, either P or Q (or both) is increased and a new optimisation procedure is initialised using previously-optimised coefficients and supplemented by new $\alpha_{p,q}$'s which are set to zero. This way we ensure that the cloaking factor $\mathcal{C}$ is set on a decreasing path. If one were to assume a classical convergence of this scheme, one might expect the increments in the degrees of freedom at each step of the optimisation to have a smaller and smaller effect on coefficients determined by the previous step and that, in this way, the optimiser finds it easy to find the new minimum at each stage of the process. However, we find this is not always the case. As the number of free variables, and hence the size of parameter space, is increased multiple local minima emerge and the global minimum can reside in a completely new part of parameter space. Thus, in practice, a combination of different strategies are used to initialise the optimisation procedure to detect the solution with the lowest $\mathcal{C}$.

5.2. *Axisymmetric beds*

In the original numerical experiments of Porter (2011) and Newman (2012) attempts to cloak using axisymmetric beds were overlooked because they were not considered likely candidates for cloaking. Whilst the best cloaking results will be shown to be associated with non-axisymmetric beds, it seems a more natural starting point to consider axisymmetric beds first. With axisymmetry, $Q = 1$ and the results are independent of the incident-wave angle β. We fix $k_0h_0 = 1$ and $a/h_0 = \frac{1}{2}$, $b/h_0 = 5$ and increase P in steps. When $P = 1$ and $\alpha_{1,1}$ is the only free weighting coefficient 1(a) shows that $\mathcal{C} < 1$ for $k_0h_0 = 1$ with $\alpha_{1,1} = 0.1$ and that there is close agreement between the MSE and FLT results. We find $\alpha_{1,1} \approx 0.11$ minimises $\mathcal{C}$ to a value of approximately 0.83. The results of the optimisation procedure for $Q = 1$ and increasing $P = 2, 4, 8$ are summarised in the first 3 lines of table 1. This table includes two calculations of $\mathcal{C}$ performed under FLT corresponding to the two definitions in the right-hand side and middle parts of equation (2.9). The difference between these two results, shown in the final column of table 1, act as an indicator of the accuracy of the results using the single precision WAMIT solver – a point we return to shortly. For FLT, we use the maximum computed value of the two

Q	P	$\mathcal{C}_{MSE}$	$\mathcal{C}_{FLT}(1)$	$\mathcal{C}_{FLT}(2)$	(1)-(2)
1	2	0.52846	0.42280	0.42315	-0.00035
1	4	0.05079	0.02343	0.02361	-0.00018
1	8	0.00086	0.00006	0.00064	-0.00058
2	2	0.18027	0.11207	0.11231	-0.00024
2	4	0.04648	0.01523	0.01534	-0.00011
2	8	6×10^{-6}	0.00008	0.00005	0.00003
4	2	0.09256	0.06425	0.06449	-0.00024
4	4	1×10^{-5}	0.00369	0.00379	-0.00010
4	8	1×11^{-11}	0.00001	0.00003	-0.00002

TABLE 1. Cloaking factors optimised under MSE and FLT with varying numbers of radial (P) and azimuthal (Q) basis modes. Here $a/h_0 = \frac{1}{2}$, $k_0h_0 = 1$, $b/h_0 = 5$. The first three lines ($Q = 1$) are axisymmetric beds. Columns labelled (1) and (2) indicate $\mathcal{C}_{FLT}$ has been computed using the first and second alternative relations of (2.9) respectively; the final column shows the difference between them.

versions of $\mathcal{E}$ defined in (2.9) as the objective function to be minimised and subsequently report just the maximum of the two versions of $\mathcal{C}_{FLT}$. From table 1 both the MSE and FLT cloaking factors are seen to decrease as P is increased. However the values of $\alpha_{p,1}$ to which the optimiser converges can be quite different, especially for larger P.

At this point we should note that the WAMIT solver which is used to implement the boundary element method for the FLT uses single precision code. The differences in the values of $\mathcal{C}_{FLT}$ computed by the two different methods shown in table 1 can be used to indicate the level of accuracy of the computations. In part this is because $\mathcal{C}$ is defined as a factor normalised by $\mathcal{E}_{cyl} = 0.090372$. Given this data is difficult to justify reporting values of $\mathcal{C}$ below values of about 0.00001.

We should also note the limitations of the MSE numerical method. Despite being written using double precision code the basis for the approximation is crude and results are dependent on the numerical discretisation (values of N, M). These can affect the coefficients found under optimisation, but these changes do not appear to significantly affect the value of $\mathcal{C}$ that is found under optimisation and we feel comfortable reporting this to 5 decimal places.

In figure 6(a)-(c) we show the radial depth profiles for cloaking-optimised axisymmetric beds under MSE and FLT for $Q = 1$, $P = 2, 4, 8$ modes, corresponding to the data in table 1. The bed profiles show reasonably good agreement for 2 and 4 radial modes. When $P = 8$ is used, the FLT finds a local minimum $\mathcal{C} = 0.0065$ when the optimiser is initialised with the MSE coefficients, which is a fairly close fit to the MSE optimised bed. However, the FLT optimiser finds a lower value of $\mathcal{C} = 0.0006$ when initialised with $P = 4$ FLT-optimised coefficients. It is believed that this represents the global minimum. In the MSE optimisation, the same minimum value is found irrespective of the initialisation of the coefficients.

Despite the superficial similarity in shape of the optimised MSE and FLT bed profiles shown in figure 6(a)-(c) the values of $\mathcal{C}$ computed from one approach using coefficients optimised under the other approach are not always so close. For example, with $Q = 1$, $P = 4$, the value of $\mathcal{C}$ computed using FLT with the coefficients optimised under MSE is 0.194, an order of magnitude higher than the optimised value of C_{FLT} shown. This illustrates the sensitivity of $\mathcal{C}$ to the bed shape and partly explains why the optimised

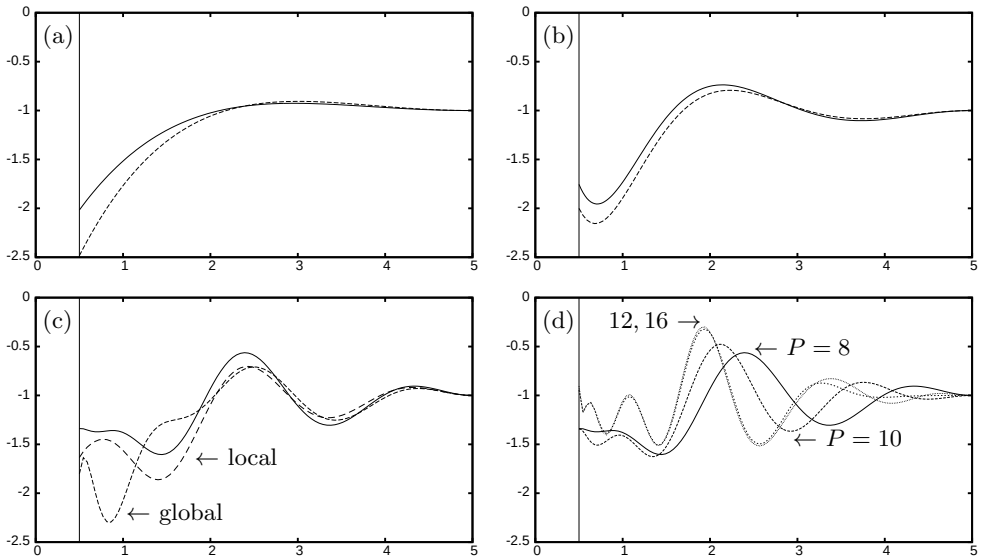

FIGURE 2. Radial depth profile of axisymmetric beds optimised under MSE (solid line) and FLT (dashed) for $Q = 1$ and: (a) $P = 2$; (b) $P = 4$; (c) $P = 8$. Axes are z/h_0 and r/h_0 with $a/h_0 = \frac{1}{2}$, $b/h_0 = 5$, $k_0h_0 = 1$. The coefficients and values of $\mathcal{C}$ are shown in table 1. In (c) local and global minima under FLT are shown. In (d) we show the MSE optimised beds for $P = 8, 10, 12, 16$.

cloaking factors and bed shapes predicted by the MSE method can appear such a long way from those computed under FLT, especially for more complicated bed shapes.

Figures 2(a)–(c) appear to indicate that the introduction of new degrees of freedom in the optimisation procedure allows the optimiser to locate completely different looking bed shapes. In figure 6(d) beds optimised under the MSE method are shown for $P = 8, 10, 12$ and 16 modes. The value of $\mathcal{C}$ drops to under 10^{-7} for $P = 12$ and less than 10^{-11} for $P = 16$. These optimised beds for larger values of P perform poorly under FLT, the increasing oscillations in the bed leading to higher bed gradients where the MSE approximation becomes less accurate. However, figure 2(d) does suggest that bed shapes do eventually converge with increasing P although it is not clear if these beds are optimised to a local minimum. Increasing P under FLT to a value of $P = 16$ reduces only slightly the optimised value of $\mathcal{C}_{FLT}$ from its $P = 8$ value. There are a number of reasons this might happen. It could be that $\mathcal{C}_{FLT}$ reaches a non-zero limit as P increases and perfect cloaking by axisymmetric beds is not possible. Or it could be that the optimiser for $P = 16$ has not found a global minimum. Or it might be that the computation of $\mathcal{C}_{FLT}$ is obscured by numerical inaccuracies.

Figure 3 shows curves of $\mathcal{C}$, for the beds optimized at $k_0h_0 = 1$, for a range of values of k_0h_0. Results are shown for the $P = 2, 4$ and $P = 8$ axisymmetric beds as displayed in figure 2. Despite having found that values of $\mathcal{C}$ are very sensitive to the bed shape, once a near-cloaking bed shape has been fixed by a minimisation of $\mathcal{C}$ for a particular wavenumber ($k_0h_0 = 1$ in these cases) the curves in figure 3 illustrate that the cloaking factor is reduced well below unity across a wide range of wavenumbers.

Next, we consider the effect of the size of the annular cloaking domain. We fix $Q = 1$ and $P = 8$ radial modes, with $a/h_0 = \frac{1}{2}$ and optimise the axisymmetric beds for cloaking at $k_0h_0 = 1$ as before. Figures 4(a,b) show the beds optimised under MSE and FLT respectively (note the vertical scales are different) for different values of b/h_0. The curves in these two figures have the same generic bed shape in the outer half of the domain

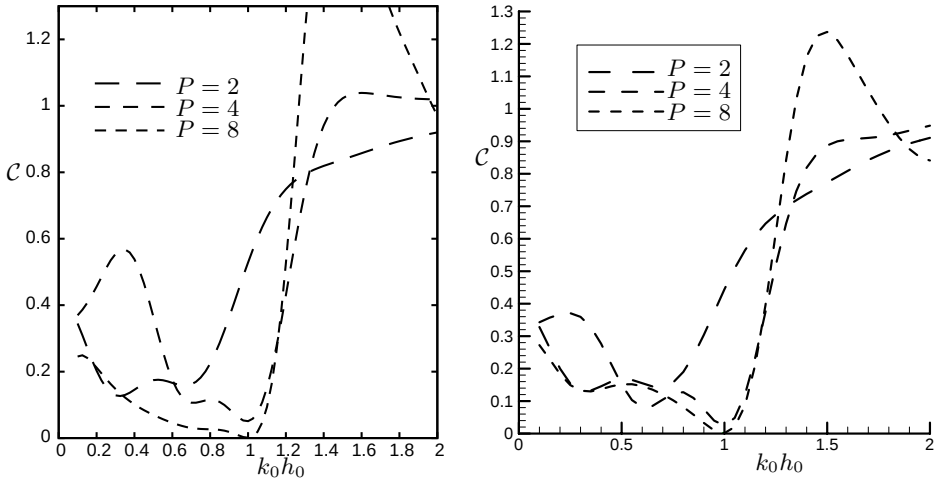

FIGURE 3. Cloaking factor against k_0h_0 for axisymmetric beds optimised by FLT with $Q = 1$, $a/h_0 = \frac{1}{2}$ $b/h_0 = 5$. Curves show varying radial modes, P.

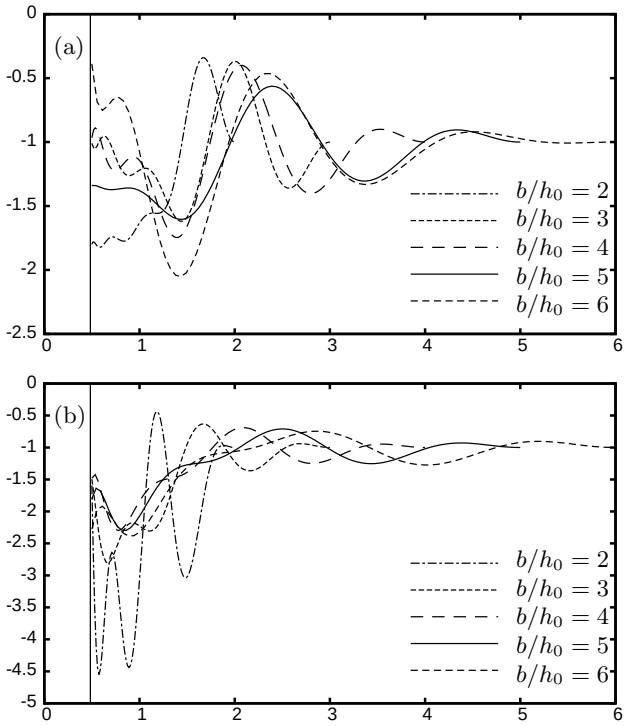

FIGURE 4. Radial depth profiles of axisymmetric beds optimised by (a) MSE and (b) FLT for $Q = 1$, $P = 8$ with $a/h_0 = \frac{1}{2}$, $k_0h_0 = 1$. In each figure the five curves represent the results using different values of the bed radius b.

although, as discussed previously, the coefficients optimised under MSE are quantitatively quite different from those optimised under FLT. The detail in the beds close to the cylinder are very different and often associated with larger bed gradients where MSE accuracy breaks down.

b/h_0	$\mathcal{C}_{MSE}$	$\mathcal{C}_{FLT}$
6	0.00590	0.02044
5	0.00086	0.00122
4	0.00002	0.00028
3	0.00029	0.00002
2	0.09840	0.01143

TABLE 2. Cloaking factors optimised under MSE and FLT for axisymmetric beds with varying cloaking domain radius, b/h_0. Here $a/h_0 = \frac{1}{2}$, $k_0h_0 = 1$, $Q = 1$, $P = 8$.

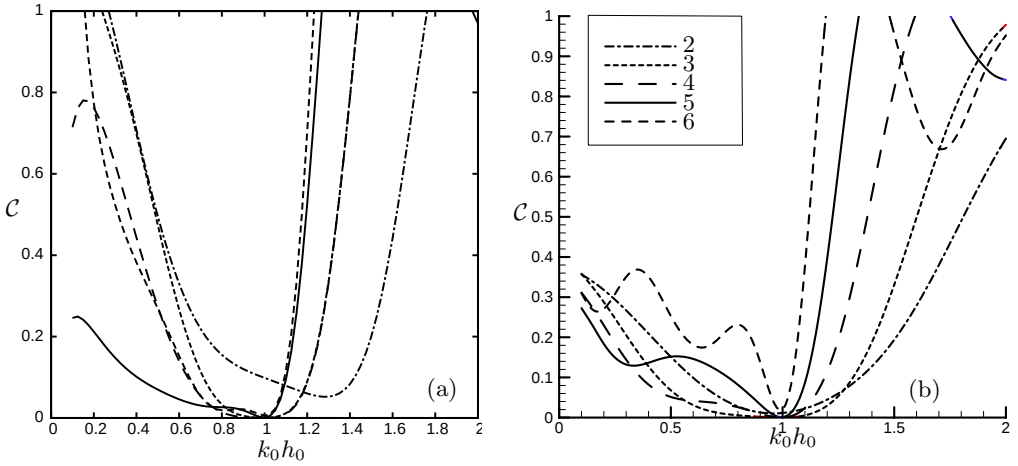

FIGURE 5. Cloaking factor against k_0h_0 for axisymmetric beds optimised by (a) MSE and (b) FLT with $Q = 1$, $P = 8$, $a/h_0 = \frac{1}{2}$. Curves show varying b/h_0.

The minimised cloaking factors associated with each of the optimised beds in figures 4(a,b) for MSE and FLT are shown in table 2. Again, cloaking factors for MSE and FLT do not show much quantitative agreement due to the sensitivity of cloaking to the model and the bed shape. However, they do share the feature that there is a minimum value of $\mathcal{C}$, in this case where the number of radial modes is fixed at $P = 8$, for a value of b/h_0 in the range from 2 to 6. In particular, the cloaking factor using FLT is reduced to a value at the practical limit of the WAMIT solver for $b/h_0 = 3$.

Figure 5 mirrors figure 3 in that it shows the variation of $\mathcal{C}$ with k_0h_0 for beds with $b/h_0 = 2, 3, 4, 5, 6$ optimised under both MSE and FLT. As before it confirms there is a reduction in $\mathcal{C}$ over a wide range of values of wavenumber.

In figure 6 the dimensionless mean drift force is plotted against k_0h_0 for the five optimised beds, from $b/h_0 = 2$ to $b/h_0 = 6$, as considered previously. The mean drift force is a second-order quantity which measures the time-averaged momentum flux on scattering surfaces and can be calculated from the first-order potential, see Mei (1983, §7.10). In particular, there is a connection between the mean drift force calculated on the scattering surfaces and the integrated far field radiated wave amplitudes (Mei (1983, §7.10, eqn 10.21)). This relation implies that perfect cloaking of the cylinder by the undulating bed translates into zero mean drift force on the combined surfaces of the cylinder and the bed. This is illustrated in figure 6(a) for curves which correspond to cloaking factors in 5(b). A reduction in the mean drift force over a wide range of wavenumbers is also evident.

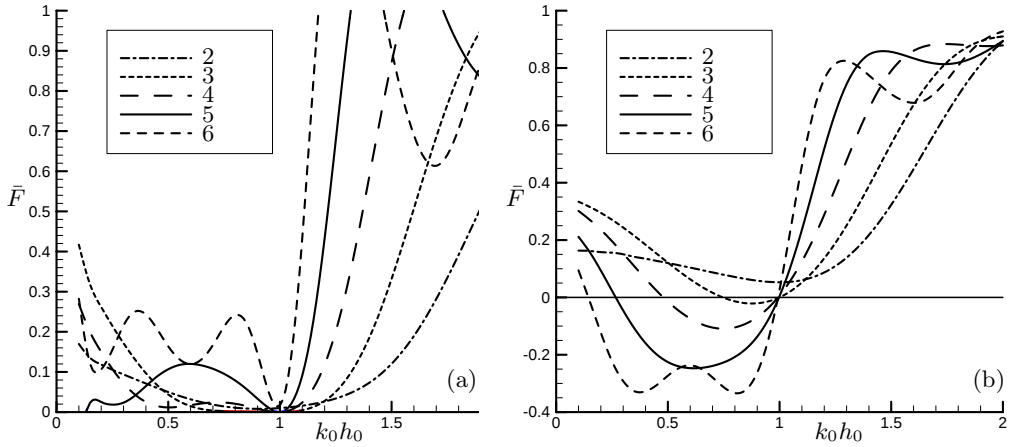

FIGURE 6. Mean drift force on (a) cylinder and varying bed and (b) cylinder only against k_0h_0 for optimised axisymmetric beds with $Q = 1$, $P = 8$, $a/h_0 = \frac{1}{2}$. Curves show varying b/h_0.

Arguably of more practical importance is the set of results in figure 6(b) which show a reduction in the mean drift force on the cylinder only with zeros of mean drift force in close correspondence to cloaking at $k_0h_0 = 1$. As in the case of the scattering energy, the total mean drift force on the cylinder and the bed is positive-definite, but the drift force on the cylinder alone can be negative as shown in figure 6(b), with a compensating positive force on the bed.

5.3. *Non-axisymmetric beds*

The results in the previous section show that the cloaking factor can be reduced to values close to zero when the bed is axisymmetric. Whilst the MSE results appear to indicate that $\mathcal{C}$ will continue towards zero as more degrees of freedom are allowed in the bed shape, the FLT results are less clear in this respect. There is certainly no obvious mathematical or physical explanation as to why perfect cloaking should be possible with purely axisymmetric bathymetry. Indeed, the low cloaking factors obtained for axisymmetric beds could be regarded as unexpected, hence the reason they were not considered in the earlier studies of Porter (2011) and Newman (2012).

We therefore continue to gather evidence for cloaking by considering non-axisymmetric beds. Our focus continues on the same example of $a/h_0 = \frac{1}{2}$, $b/h_0 = 5$ and cloaking at $k_0h_0 = 1$, but now $Q > 1$.

In particular, combinations of values of $P = 2, 4, 8$ and $Q = 2, 4$ have been considered using both the MSE and FLT. The objective for each set of values of (Q, P) considered is to find the lowest valid value of $\mathcal{C}$ using different initial values of the coefficients $\alpha_{p,q}$. These initial values were chosen in many different ways to attempt to find the lowest minimum. One approach uses previously optimised sets of coefficients with smaller values of Q or P (or both). Another uses the MSE-optimised coefficients to initialise an optimisation for the FLT. Occasionally the best results were found by initialising $\alpha_{p,q} = 0$ for all p, q. The results also had to be carefully analysed. In some cases, optimisation of $\mathcal{C}$ corresponding to large values of $\alpha_{p,q}$ which describe beds with large amplitude oscillations. In other cases, the optimised beds would approach the free surface and the optimisation is stopped.

Results for non-axisymmetric beds are tabulated in the lower section of table 1. Both the MSE and FLT show that the extra degrees of freedom in the bed provided by angular

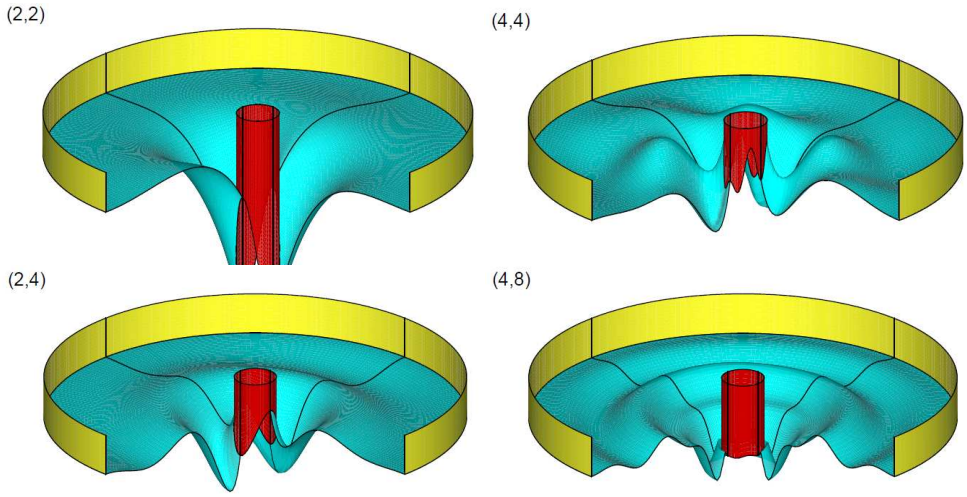

FIGURE 7. Perspective views with cut-aways of non-axisymmetric beds optimised under FLT. The outer cylinder in each figure is the matching boundary S_m as defined in Section 4. Values of (Q, P) are shown in brackets. Here $a/h_0 = \frac{1}{2}$, $b/h_0 = 5$, $k_0 h_0 = 1$.

variations lead to a reduction in the cloaking factor. This reduction is generally much more modest with increasing Q than was found with increasing P.

Bearing in mind the reservations set out concerning the accuracy of FLT computations, the results for $(P, Q) = (2, 8)$ and (4.8) in table 1 do seem to provide a stronger indication that perfect cloaking is possible. As mentioned above, the value of 0.00001 is at the limits of the estimated accuracy of the FLT code, and it is not possible to say whether the true value may actually be even smaller than this.

Figures 7 shows four bed shapes with the same dimensions, which are optimised using FLT. The number of Fourier/Chebyshev coefficients and minimum value of $\mathcal{C}$ are shown for each bed. The cylinder is shown in red in the centre of each plot, which is cut away to show the profiles of the beds (shown in blue) in the $\theta = 0$ and $\theta = \frac{1}{2}\pi$ planes. The outer yellow boundary is not a physical boundary but the boundary over which the inner and outer regions are matched in the boundary integral method. It coincides with the outer circle of radius b.

Further numerical experiments carried out, but not reported here, consider cloaking for different values of a/h_0 and $k_0 h_0$. It is found that the optimisation procedure of cloaking described here is robust to changes in these values. As $k_0 a$ is reduced below the value of unity considered in this paper, cloaking factors reduce towards zero faster with increasing Q, P and vice versa. The undulating bathymetry acts to scatter waves in order to deconstructively interfere with the waves scattered by the cylinder. For lower values of $k_0 a$ the scattering by the cylinder is dominated by the coefficients of the lower Fourier mode expansion in θ. Thus, it is perhaps not surprising that the undulating bed needs less refinement.

6. Conclusions

Numerical evidence has been provided showing that the incident wave energy scattered in diffracted waves by a vertical cylinder over a flat sea bed can be reduced towards zero when the bathymetry in an annular region outside the cylinder is allowed to vary. Results

presented here have focussed mainly on axisymmetric beds where this 'cloaking effect' is independent of incident wave direction and where bed profiles are easier to compute, visualise and possibly construct in an experiment. Two approaches have been described, the first approximate and based on an implementation of the depth-averaged modified mild-slope equations. Numerical optimisation results from this approximation are then used as initial guesses in a method based on full three-dimensional linearised theory. This has required a modification to the boundary-element code WAMIT to account for depressions in the annular cloaking region below the depth of the bed at infinity. In the best example of cloaking under full linear theory we have produced a reduction in the total scattering cross section of 10^{-5} over that for a cylinder on a flat bed. This computation is at the practical limit of the program accuracy and it is tempting to conclude that the cloaking factor could be reduced indefinitely towards zero with increasing refinement in the bed shape.

The focus here has been on one particular example of cylinder size a/h_0 and wavelength $k_0h_0 = 1$. With these fixed values, it has been shown that near-cloaking occurs for different sizes of the cloaking region b/h_0, in each case with the scattered energy reducing towards zero as the description of the bed shape is increased in refinement. Within these values there is evidence that there are particular values of b/h_0 which minimise the scattering cross section at a faster rate with increasing modes describing the bed. It could have been possible to include b/h_0 as an additional free parameter in the optimisation procedure to further refine the cloaking process.

It has also been shown that the mean drift force on the cylinder is greatly reduced by cloaking-optimised beds in a wide range of frequencies around the cloaking frequency. This could have some practical significance in the design, for example, of offshore wind turbine foundations.

Further work on cloaking being investigated includes replacing the varying bed by other scattering obstacles (Newman (2013)). The use of optimisation routines to design marine structures having particular characteristics could be useful in other applications, for example in wave energy capture (e.g. Kurniawan & Moan (2012)).

REFERENCES

Alam M., 2012, Broadband claoking in Stratified Seas *Phys. Rev. Lett.* **108**, 084502.

Alù, A. & Engheta, N., 2005, Achieving transparency with plasmonic and metamaterial coatings. *Phys. Rev. E* **72**, 016623 (9 pages).

Belibassakis K.A., 2008, A boundary element method for the hydrodynamic analysis of floating bodies in variable bathymetry regions *Eng. Anal. with Boundary Elements* **32**, 796–810.

Chamberlain, P.G. & Porter, D., 1995 The modified mild-slope equation. *J. Fluid Mech.* **291**, 393–407.

Chamberlain, P.G. & Porter, D., 1999 Scattering and near-trapping of water waves by axisymmetric topography. *J. Fluid Mech.* **388**, 335–354.

Chen H. & Chan C.T., 2007, Acoustic cloaking in three dimensions using acoustic metamaterials. *Appl. Phys. Lett.* **91**(19), 183518 (3 pages).

Cummer A. & Schurig D., 2007, One path to acoustic cloaking. *New J. Phys.* **9**, 45.

Cummer, S.A., Popa, B-I., Schurig, D., Smith, D.R., Pendry, J.B., Rahm, M. & Starr, A., 2007, Scattering theory derivation of a 3D acoustic cloaking shell. *Phys. Rev. Lett* **100**, 024301.

Ehrenmark, U., 2005, An alternative dispersion equation for water waves over an inclined bed *J. Fluid Mech.* **543**, 249–266.

Farhat, M., Guenneau, S., Enoch, S. & Movchan, A. B., 2009, Cloaking bending waves propagating in the elastic plates. *Phys. Rev. B.* **79**(4), 033102.

Farhat M., Enoch S., Guenneau S. & Movchan A. B., 2008, Broadbanded cylindrical acoustic cloak for linear surface waves in a fluid. *Phys. Rev. Lett.* **101**, 134.

Ferreira, M.D. & Newman, J.N., 2009, Diffraction effects and ship motions on an artificial seabed. *Proc. 24th Int. Workshop on Water Waves and Floating Bodies, Zelenogorsk, Russia.*

Griffiths, L. S. & Porter, R., 2012, Focusing of surface waves by variable bathymetry. *Appl. Ocean Res.* **34**, 150–163.

Lee, C.-H. & Newman, J.N., 2004, Computation of wave eects using the panel method. In *Numerical Modeling in Fluid-Structure Interaction*, Ed. S. Chakrabarti. WIT Press.

Leonhardt, U., 2006, Optical conformal mapping *Science* **312**, 1777–1780.

Liu H.-W., Wang, Q.-Y. & Tang, G.-T., 2013, Exact Solution to the Modied Mild-Slope Equation for Wave Scattering by a Cylinder with an Idealized Scour Pit. *J. Waterway Port, Coastal & Ocean Eng.* (to be published) doi:10.1061/(ASCE)WW.1943-5460.0000195

Kurniawan, A. & Moan, T., 2012, Multi-objective optimization of a wave energy absorber geometry In *Proc 27th Int. Workshop on Water Waves and Floating Bodies*, Copenhagen, Denmark.

Maruo, H., 1960, The drift force of a body floating in waves. *J. Ship Res.* **4**, 1–10.

Mei, C.C., 1983, *The applied dynamics of ocean surface waves.* Wiley Interscience.

Milton, G. W., Briane, M. & Willis, J. R., 2006, On cloaking for elasticity and physical equations with a transformation invariant form. *New J. Phys.* **8**, 248.

Newman, J.N., 2012, Scattering by a cylinder with variable bathymetry. In *Proc 27th Int. Workshop on Water Waves and Floating Bodies*, Copenhagen, Denmark.

Newman, J.N., 2013, Cloaking a circular cylinder in water waves. *Submitted to Euro. J. Mech. Fluids B.*

Pendry J. B., Schurig D. & Smith D. R., 2006, Controlling electromagnetic fields. *Science* , **312**, 1780–1782.

Pinkster, J.A., 2011, A multi-domain approach in 3-D diffraction calculations. *30th Int. Conf. on Ocean, Offshore and Arctic Eng., Rotterdam, Netherlands. (OMAE2011-49414).* 355–364.

Porter, R., 2011 Cloaking a cylinder in waves. In *Proc 26th Int. Workshop on Water Waves and Floating Bodies*, Athens, Greece.

Porter, R. & Porter, D., 2001 Interaction of water waves with three-dimensional periodic topography. *J. Fluid Mech.* **434**, 301–335.

Ward A.J. & Pendry J.B., 1996, Refraction and geometry in Maxwell's equations *J. Mod. Opt.* , 773–793.

Wehausen, J.V. & Laitone, E.V.(1963) Surface Waves. In *Handbuch der Physik*, (Ed. S. Flugge), Vol. 9. Berlin: Springer-Verlag, pp. 446–778.